Comparison of Pt and Ag as co-catalyst on g-C$_3$N$_4$ for improving photocatalytic activity: Experimental and DFT studies

Kezhen Qi[a,b], Shu-yuan Liu[c,*], Rengaraj Selvaraj[d,*], Wei Wang[e], Zhaoxiong Yan[f,*]

[a]*Institute of Catalysis for Energy and Environment, College of Chemistry and Chemical Engineering, Shenyang Normal University, Shenyang 110034, China, email: qkzh2003@aliyun.com (K. Qi)*
[b]*State Key Laboratory of Photocatalysis on Energy and Environment, Fuzhou University, Fuzhou, 350116, China*
[c]*Department of pharmacology, Shenyang Medical College, Shenyang 110034, China, email: liushuyuan@symc.edu.cn (S.-Y. Liu)*
[d]*Department of Chemistry, College of Science, Sultan Qaboos University, Muscat 123, Oman,*
email: srengaraj1971@yahoo.com (R. Selvaraj)
[e]*School of Chemistry and Chemical Engineering, Shihezi University, Shihezi, 832000, China, email: wangw@shzu.edu.cn (W. Wang)*
[f]*Key Laboratory of Optoelectronic Chemical Materials and Devices of Ministry of Education, and Hubei Key Laboratory of Industrial Fume and Dust Pollution Control, Jianghan University, Wuhan 430056, China, email: zhaoxiongyan75@163.com (Z. Yan)*

ABSTRACT

In this work, Ag and Pt were compared as a co-catalyst on graphitic carbon nitride (g-C$_3$N$_4$) for the enhanced photocatalytic activity of water splitting into hydrogen generation. In order to prepare Ag/g-C$_3$N$_4$ and Pt/g-C$_3$N$_4$, initial adsorption of noble metal ions was performed on the g-C$_3$N$_4$ surface, followed by reducing them by using NaBH$_4$. Decoration of Ag or Pt nanoparticles on g-C$_3$N$_4$ can extend the visible light adsorption and promote segregation of the photogenerated carriers, which contribute to an improved photocatalytic performance. Pt/g-C$_3$N$_4$ has a higher photocatalytic activity in water splitting for H$_2$ generation (841 µmol g^{-1} h^{-1}) than that of Ag/g-C$_3$N$_4$ (305 µmol g^{-1} h^{-1}), however, almost no H$_2$ generation for pure g-C$_3$N$_4$. For checking the photogenerated holes, •OH generation rate was tested by using the reaction of terephthalic acid (TA) with •OH to form 2-hydroxyterephthalic acid (TAOH). On the basis of experimental results and theoretical calculation, a possible photocatalytic mechanism is put forward. It is suggested that Pt can play a better role as the co-catalyst than Ag can, due to the d-centre of Pt is closer to Fermi level than that of Ag on the g-C$_3$N$_4$ surface, which can promote the charge separation and accelerate the electron transformation.

Keywords: g-C$_3$N$_4$; Ag or Pt loading; Photocatalytic; Water splitting; DFT calculation

1. Introduction

Environmental pollution and energy crisis have brought a threat to human survival [1–12]. It is urgent to develop a green and renewable energy, for example, hydrogen energy [13–20]. Photocatalytic water splitting to produce hydrogen that uses of the solar energy and water is one of the most advanced technology [21–28]. Graphitic carbon nitride (g-C$_3$N$_4$), being a promising photocatalyst, has gotten the worldwide attention, due to its satisfaction of the fundamental needs for the water-splitting, because of its suitable

positions of conduction band (CB) and valence band (VB) [29–34]. Nevertheless, g-C$_3$N$_4$ possesses only a weak photocatalytic activity for hydrogen generation, owing to the low usage of solar energy and the fast recombination of photogenerated charge carriers.

The deposition of noble metals as co-catalysts on the photocatalyst surface is an effective way to enhance the photocatalytic activity in many cases [35–37]. The deposited noble metals mainly have two functions, one is to promote the segregation of photogenerated carriers, another is to be worked as the reaction active sites [38–40]. For example, Maeda et al. loaded g-C$_3$N$_4$ with Pt, Pd and Au to improve the photocatalytic performance of water splitting into

*Corresponding author.

hydrogen generation [41]. The results shows that the photocatalytic performance of g-C_3N_4 is extensively enhanced after the decoration of noble metals, especially, with Pt decoration [42]. Although the g-C_3N_4-based photocatalysts with Pt and Ag as the co-catalyst have very successfully been put in use for the photocatalytic water splitting, the systematical investigation on the comparison of these two co-catalysts of Pt and Ag for enhancing the activity of g-C_3N_4 is very few.

In this work, preparation of g-C_3N_4 samples with Ag and Pt loading has been performed by the methods of the pyrolysis of urea and liquid-phase reduction of noble metal ions. After Ag or Pt loading, the photocatalytic efficiency of g-C_3N_4 regarding water splitting is obviously improved. The photocatalytic activity for water splitting for Pt/g-C_3N_4 is much greater than that of Ag/g-C_3N_4. The generation rate of holes on Pt/g-C_3N_4 is faster than that on Ag/g-C_3N_4, as monitored by the generation rate of ·OH. The supreme of loading of Pt nanoparticles (NPs) on g-C_3N_4 than that of loading Ag can be explicated with the enhanced visible light response and the speeding up of the segregation of the photogenerated carriers. On the basis of the density functional theory (DFT) calculation and experimental results, a possible photocatalytic mechanism is proposed, and the underlying reason that Pt is a better co-catalyst than Ag, is that d-centre of Pt is closer to Fermi level than that of Ag on the g-C_3N_4 surface, that accelerates the charge separation and electron transformation.

2. Experimental

2.1. Photocatalyst synthesis

The g-C_3N_4 nanosheets were prepared by a method of thermal polycondensation of urea. 15 g urea was placed into a covered ceramic crucible, followed by heating at 500°C for 5 h in air with the heating rate of 10°C/min. After reaction, the product naturally cooled down to the room temperature, followed by grinding to the powder. Ag/g-C_3N_4 was prepared by a liquid-phase reduction method. First, 0.5 g of g-C_3N_4 powder was put in 50 mL water, and ultrasonic treating for 5 min. Second, a specific amount of $AgNO_3$ (5 mM) aqueous solution was put into the above g-C_3N_4 suspension solution, maintained stirring. Third, dissolution of a specific quantity of $NaBH_4$ (the molar ratio of n(Ag-NO_3):n($NaBH_4$) = 1:5) was made into H_2O amounting to 30 mL, and then put into the solution mentioned above, and stirred it for1 h. Finally, the product was centrifuged and then its washing was done using the absolute ethanol and purified water, which proceeded to drying in the vacuum oven at a temperature of 70 °C for 5 h. The sample, with the ratio of Ag and g-C_3N_4 is 3%, was prepared and labelled as Ag/g-C_3N_4. For synthesizing the same amount of Pt loading (3%) as Ag loading on g-C_3N_4, i.e. Pt/g-C_3N_4, a similar procedure as done for Ag/g-C_3N_4 was followed except that $AgNO_3$ was replaced by $H_2PtCl_6·6H_2O$.

2.2. Characterizations

Examination of the crystal phase of products was carried out by using the X-ray diffraction (XRD) (Bruker D5005 X-ray diffractometer, Cu Kα, and λ = 1.54056 Å). Fourier transform infrared (FTIR) spectra were conducted by a Nicolet Magna 560 spectrophotometer. X-ray photoelectron spectroscopy (XPS) was carried out on a PHIQ uantum1600 XPS instrument. The high resolution transmission electron microscopy (HRTEM) was measured by using a JEOL JEM-2100F electron microscope. Collection of the UV–vis absorbance spectra was conducted on a Shimadzu UV-3100 spectrophotometer, which made use of $BaSO_4$ as a reference. Investigations of the photoluminescence (PL) spectra of g-C_3N_4 and Ag/g-C_3N_4 samples were carried out on a Varian Cary Eclipse spectrometer, which had an excitation wavelength amounting to 325 nm.

2.3. Photocatalytic activity

The photocatalytic water splitting for H_2 production was carried out in a Pyrex flask with a volume of 100 mL that had 3 openings under the seal of rubber plugs. The simulated sunlight source was shining from a 350 W Xe lamp, the distance between the reaction solution and lamp is 15 cm. 10 mg photocatalyst was dispersioned into an aqueous solution amounting to 80 mL that contained 10 ml triethanolamine under continuous magnetic stirring. Before irradiation, the reaction solution was bubbled by N_2 for 30 min to remove air. Sampling of the photocatalytic generated H_2 was carried out by 0.4 mL gas from the reaction system, followed by the analysis by a gas chromatograph (GC-14C, Shimadzu, Japan, TCD , N_2 was put to use as the carrier gas).

2.4. Photoelectrochemical property

The photoelectrochemical efficiency was investigated on a CHI 660D electrochemical work station by means of a standard 3-electrode system. g-C_3N_4, Ag/g-C_3N_4 and Pt/g-C_3N_4 were put on the ITO glass surface, respectively, as the functional electrode. Pt wire and a calomel electrode were used as the counter electrode and reference electrode, respectively. The electrolyte amounts to 0.1 mol/L Na_2SO_4 aqueous solution. An amount of 5 mg photocatalysts was mixed with 1 mL quantity of ethanol, subsequently coating of the mix on 2 cm × 4 cm ITO glass in order to utilize as an electrode.

2.5. DFT calculation

All calculation is carried out by VASP package software [43,44]. The generalized gradient estimation is used by means of the functional of Perdew and Wang (GGA-PW91) [45]. Description of the electron-ion interaction is performed using the projector-augment wave (PAW) scheme [46,47], with regard to the plane wave set, the cutoff energy of 450 eV was used in calculation. A Pt or Ag cluster contained four atoms was put in a $30×30×30 Å^3$ box. In calculation, all the four atoms are allowed to relax. Spin-polarized computations were carried out as required. With regard to the integration in the Brillouin region, the Monkhorst-Pack [48] meshes of (3×3×3) was used. The d-band center (μ_d^c) is used to study the electronic structure of the pristine tetrahedral Ag or Pt cluster, which can be calculated by the formula:

$$\mu_d^c = \frac{\int_{-\infty}^{E_F} E \cdot \rho_d(E)dE}{\int_{-\infty}^{E_F} \rho_d(E)dE},$$

where ρ_d represents the density of states projected onto the d-band.

3. Results and discussion

3.1. XRD

As confirmed by the XRD data (Fig. 1), graphite carbon nitride (g-C_3N_4, JCPDS87-1526) was formed. The peaks at 13.1° and 27.5° correspond to the (100) and (002) facets of g-C_3N_4, respectively. The peak at 13.1° corresponds to the in-plane structural packing theme of the tris-triazine units. The peak at 27.5° is in line with the interlayer loading of the fragrant segments [49]. Moreover, because no apparent diffraction peak of Pt or Ag over g-C_3N_4 appeared, these two noble metals should exist as small NPs and extremely disseminate on the surface of g-C_3N_4 [36]. Among these three samples, the intensity and position of the related XRD diffraction peaks did not show obvious difference, suggesting that the loading of Ag and Pt metals did not make any changes on the g-C_3N_4 structure.

3.2. FTIR

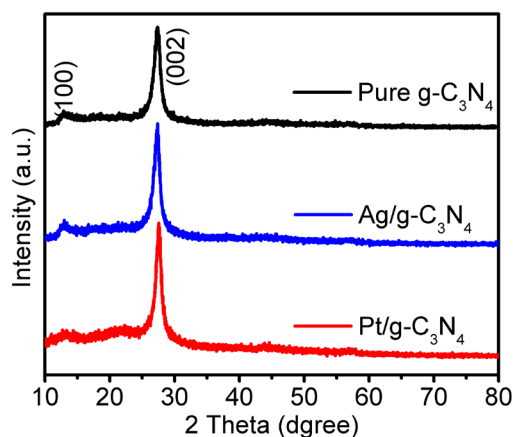The chemical structure of as-prepared samples was carried out by using FTIR measurement (Fig. 2). The peak at
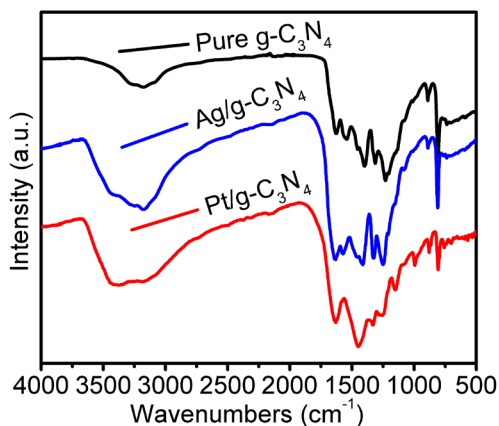
1639 cm^{-1} is ascribed to the stretching vibration C-N groups. The peaks at 1249, 1319 and 1433 cm^{-1} are assigned to the fragrant C-N stretching vibration [50]. The peak at 804 cm^{-1} is in line with the breathing manner of the triazine units [51]. The peak at 3255 cm^{-1} is attributed to stretching vibration of N-H group [52]. The FTIR spectra of the g-C_3N_4 sample show no apparent difference after loading of Pt and Ag, which indicates that both the Pt and Ag loading have not changed the layer stucture of g-C_3N_4, which is consistent with the XRD result.

3.3. UV-DRS

Fig. 3 shows the UV-vis absorbance spectra of the as-prepared samples. For pure g-C_3N_4, the location of the absorption edge is at 440 nm that is consistent the band gap of the bulk g-C_3N_4 (2.8 eV) [53]. On the deposit of Ag or Pt on the surface of g-C_3N_4, the absorption edges show a redshift. In comparison with pure g-C_3N_4, both the Pt/g-C_3N_4 and Ag/g-C_3N_4 samples show an apparent absorption in the visible light region. Compared with pure g-C_3N_4, Ag/g-C_3N_4 has an additional weak and a wide absorption peak at 450–600 nm that constitutes the attribute of the silver surface plasmon resonance (SPR) band [54].

3.4. Photoluminescence

In order to study the effect of Ag and Pt loading on the segregation of photogenerated electrons and holes, the PL measurement was performed (Fig. 4). All samples show a wide PL peak between 420 and 500 nm, centered at 460 nm, which is attributed to the band-band PL mechanism and the energy of light almost equivalents to the band-gap energy of g-C_3N_4. Interestingly, after the deposition of Ag or Pt, a declination of PL intensity is observed, which indicates that an enhancement in the separation rate of the photogenerated carriers is realized. In addition, the Pt/g-C_3N_4 sample shows the lower PL intensity than that of Ag/g-C_3N_4 and of pure g-C_3N_4. This greater segregation effectivity of the photogenerated carriers in the Pt/g-C_3N_4 sample is expected to cause an enhanced photocatalytic activity.

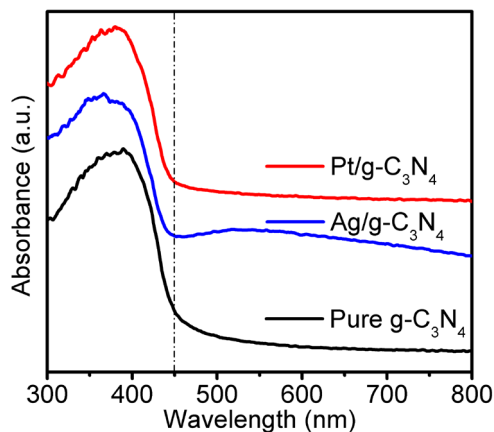Fig. 1. XRD patterns of the pure g-C_3N_4, Ag/g-C_3N_4 and Pt/g-C_3N_4 samples.

Fig. 2. FTIR spectra of the pure g-C_3N_4, Ag/g-C_3N_4 and Pt/g-C_3N_4 samples.

Fig. 3. UV-vis DRS spectra of the pure g-C_3N_4, Ag/g-C_3N_4 and Pt/g-C_3N_4 samples.

3.5. Morphologies analysis

Figs. 5A and 5B show typical TEM images of Ag/g-C_3N_4 and Pt/g-C_3N_4, respectively. Both the Ag and Pt NPs have a homogenous dispersion on the surface of g-C_3N_4 nanosheets. The size distribution of the Ag and Pt NPs has been calculated, which have been presented in Figs. 5C and 5D, respectively. Regard to the size of depositing NPs on the g-C_3N_4 surface, the Pt NPs is between 3 and 8 nm, while the Ag NPs is in the range of 8–18 nm. The Ag and Pt NPs
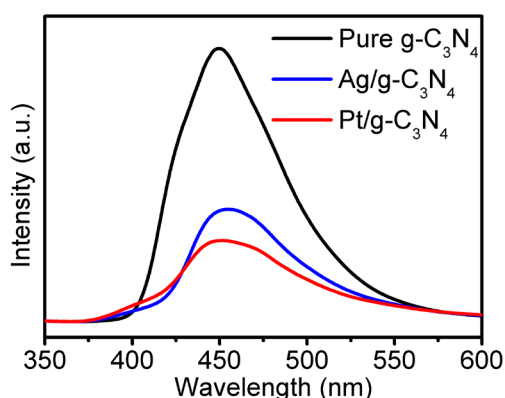
Fig. 4. PLspectra of the pure g-C_3N_4, Ag/g-C_3N_4 and Pt/g-C_3N_4 samples.

can function as the active sites in catalytic reaction process, which will promote the photocatalytic reaction.

3.6. Surface chemical states

XPS measurement was used to study the surface chemical compositions of the as-prepared samples. Fig. 6A shows the XPS survey spectra of the pure g-C_3N_4, Pt/g-C_3N_4 and Ag/g-C_3N_4 samples. As revealed by the XPS survey spectra of the Pt/g-C_3N_4 and Ag/g-C_3N_4 samples, there are strong signals from Pt and Ag, respectively, which reveal that loading of both Ag and Pt is successfully performed on the g-C_3N_4 surface. As shown in Figs. 6B and 6C, the structures of the high-resolution XPS of C and N on the samples show no apparent variation after loading of Ag and Pt, which suggests that the integrity of attribute layer structure of g-C_3N_4 is kept, without being impacted by the Ag or Pt modification. Nevertheless, it is observed that both the C 1s and N 1s binding energies are moved towards an higher binding energy than the pure g-C_3N_4, that is ascribed to the existence of a strong interfacial contact between the Ag and Pt with g-C_3N_4 that is capable of increasing the transfer of the charge [55]. The spectrum of Ag 3d has been shown in Fig. 6D. It is assigned the peaks at 367.4 eV and 374.0 eV as Ag $3d^{5/2}$ and Ag $3d^{3/2}$ [56,57]. This validates that Ag NPs are effectively coasting on the g-C_3N_4 surface. With regard to the Pt 4f XPS spectra (Fig. 6D), the 2 peaks are located at binding energy of 71.11 and 74.30 eV that are indexed as Pt 4f7/2 and Pt 4f5/2, respectively, indicating that it is the
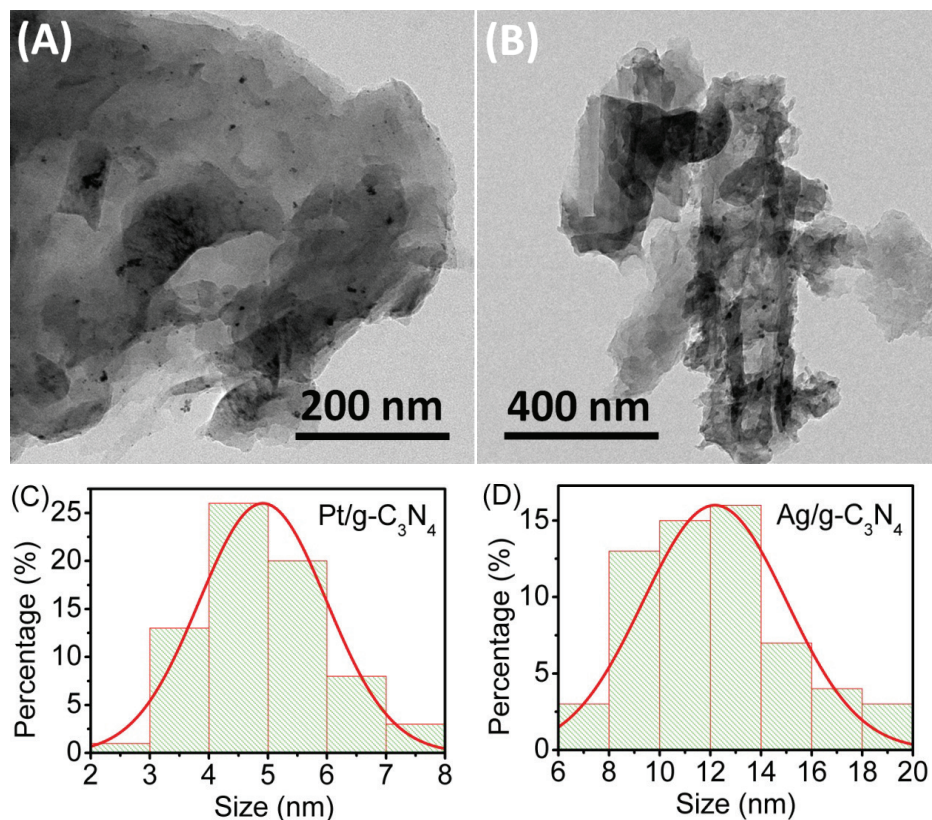
Fig. 5. TEM images of (A) Pt/g-C_3N_4 and (B) Ag/g-C_3N_4, corresponding the size distribution of Pt NPs (C) and Ag NPs (D).
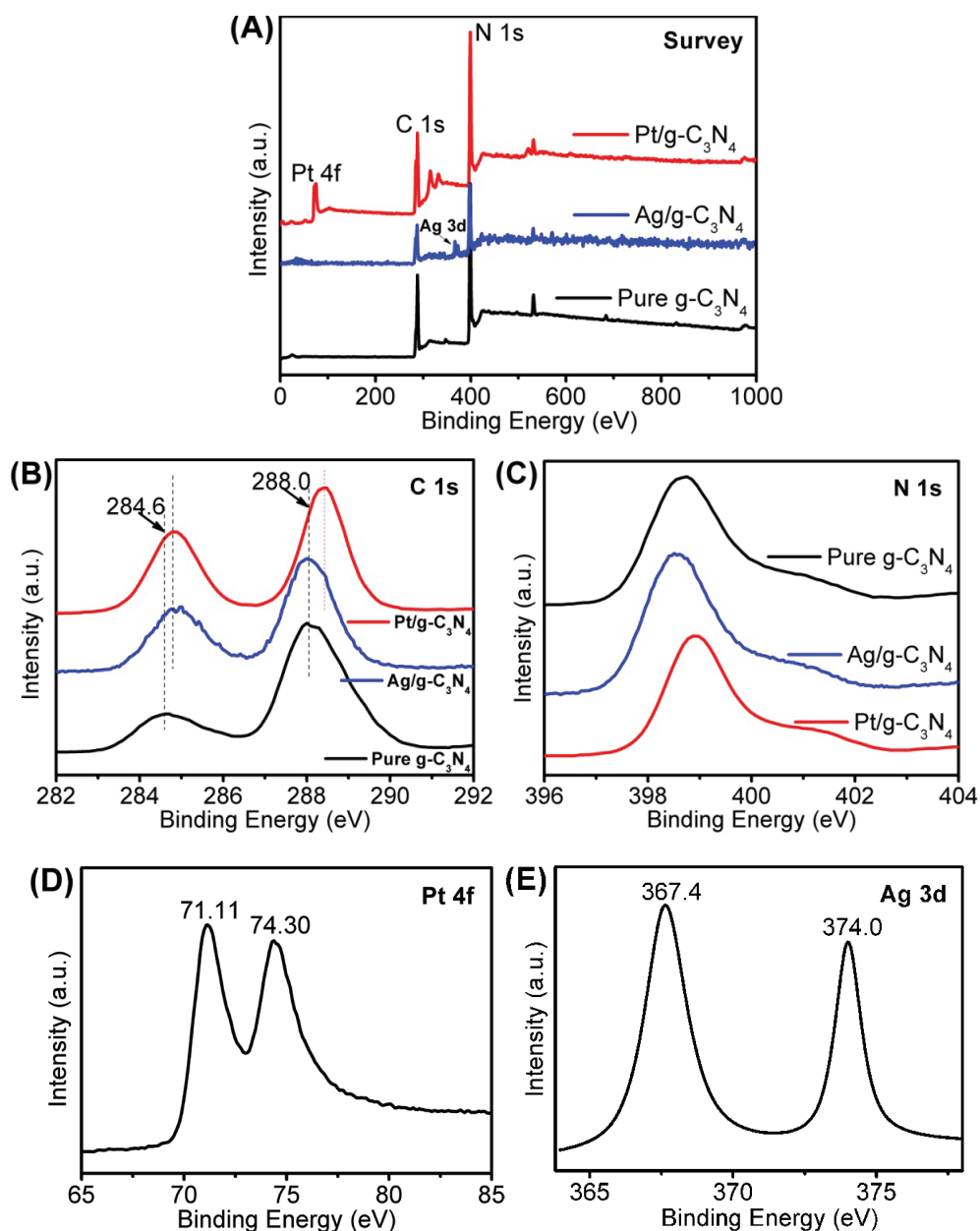
Fig. 6. XPS spectra of Ag/g-C$_3$N$_4$ composites: survey XPS spectrum (A), high resolution of C 1s (B), N 1s (C), Pt 4f (D) and Ag 3d (E) spectrum.

metallic Pt which is on the g-C$_3$N$_4$ surface [58]. Based on the XPS analysis, it is confirmed that the Pt and Ag NPs are adsorbed on the g-C$_3$N$_4$ surface.

3.7. Photocatalytic water splitting

The photocatalytic activity test is carried out through water splitting into hydrogen generation under the simulated sunlight irradiation. Fig. 7 shows the H$_2$ production over the pure g-C$_3$N$_4$, Ag/g-C$_3$N$_4$, Pt/g-C$_3$N$_4$ samples under the irradiation for 5 h. There is almost no hydrogen production for pure g-C$_3$N$_4$. Pt/g-C$_3$N$_4$ (841 μmol g^{-1} h^{-1}) has a higher photocatalytic activity of H$_2$ production than that of

Ag/g-C$_3$N$_4$ (305 μmol g^{-1} h^{-1}). After the loading of Ag and Pt on the surface of g-C$_3$N$_4$, the hydrogen yield has been substantially increased, which is due to the formation of Schottky barrier between the noble metal and g-C$_3$N$_4$ that has been effectively promoting the segregation of photogenerated carriers.

3.8. Hydroxyl radical generation

The reaction of terephthalic acid (TA) to the 2-hydroxyterephthalic acid (TAOH) is an useful method for the investigation of the hydroxyl radical (•OH) generation rate [59]. In this work, the reaction solution is constituted by 3
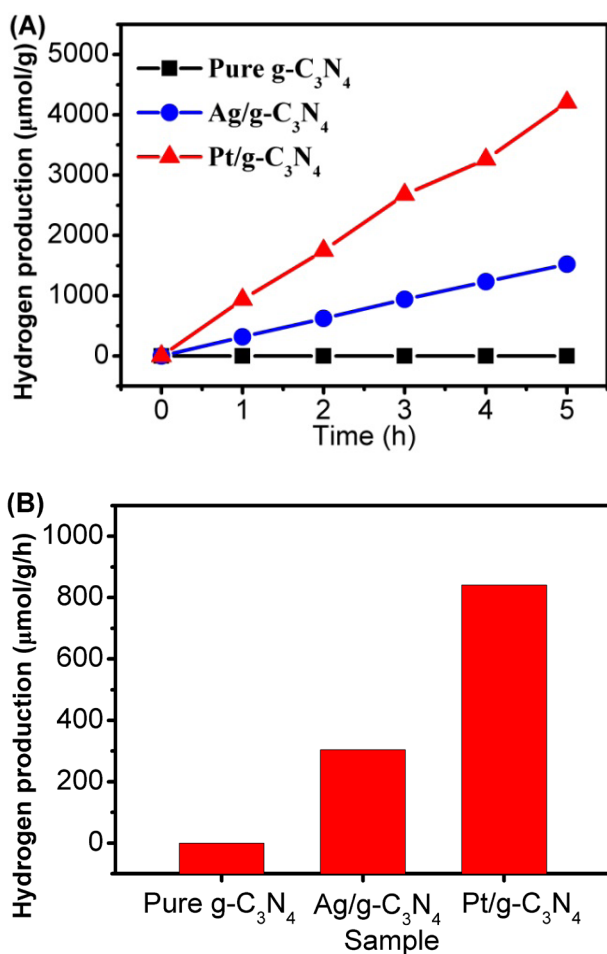
Fig. 7. (A) Plots of photocatalytic hydrogen evolution under simulated sunlight irradiation for different photocatalysts within 5 h, (B) Comparing hydrogen evolution rate for the pure g-C$_3$N$_4$, Ag/g-C$_3$N$_4$ and Pt/g-C$_3$N$_4$photocatalysts.

Fig. 8. Photocatalyticly TA reacts with •OH to form TAOH by pure g-C$_3$N$_4$, Ag/g-C$_3$N$_4$ and Pt/g-C$_3$N$_4$ under the same simulated sunlight irradiation.
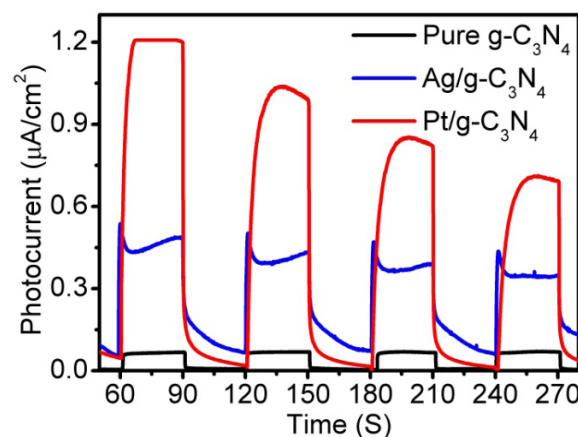
Fig. 9. Photocurrent response of pure g-C$_3$N$_4$, Ag/g-C$_3$N$_4$, and Pt/g-C$_3$N$_4$samples.

mmol/L TA and 10 mmol/L NaOH. The simulated sunlight is used as light source. Under the irradiation, TA is capable of reacting with •OH and forming TAOH, TAOH can generate fluorescence at an emission band at λ_{max} = 425 nm by the excited light of λ_{exc} = 315 nm. TAOH concentration is monitored in a range of 30 min (Fig. 8). It is known that •OH generates from h$^+$ reacted with OH$^-$. So, the reaction TA to TAOH is tested for checking the •OH generation rate, which can in turn reflect the h$^+$ generation rate. Pt/g-C$_3$N$_4$ shows a higher •OH generation rate than that of pure g-C$_3$N$_4$ and Ag/g-C$_3$N$_4$. The loading of Pt NPs on g-C$_3$N$_4$ promotes the OH$^-$ oxidation by photogenerated holes. Pt/g-C$_3$N$_4$ shows a greater activity than that of g-C$_3$N$_4$, and enhanced the efficiency of •OH formation.

3.9. Photoelectric response

The photogenerated e$^-$–h$^+$ separation efficiency of pure g-C$_3$N$_4$, Ag/g-C$_3$N$_4$ and Pt/g-C$_3$N$_4$ is studied by the photoelectrochemical tests. Under the simulated sunlight irradiation, the photocurrent response is measured over four on-off cycles, as presented in Fig. 9. The photocurrent value
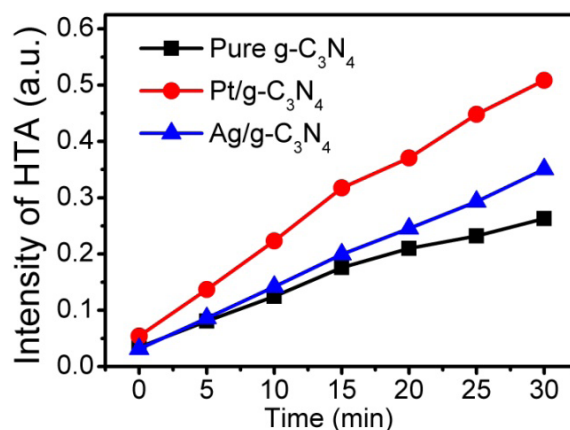
is zero when the light is turned off, and the photocurrent restarts again on turning on the light. Pt/g-C$_3$N$_4$ shows the largest photocurrent density (~0.9 μA/cm^2) among these three samples, which is higher than that of pure g-C$_3$N$_4$ (0.07 μA/cm^2) and that of Ag/g-C$_3$N$_4$ (0.5 μA/cm^2). The higher photocurrent value comes from the better performance of charge segregation in Pt/g-C$_3$N$_4$. The greater segregation effectivity of the photogenerated e$^-$–h$^+$ pair for Pt/g-C$_3$N$_4$ is in good agreement with its higher photocatalytic activity regarding to the hydrogen generation and •OH formation.

3.10. DFT calculation

The electronic structure difference between Ag and Pt cluster was investigated by the DFT calculation. Hammer et al. [60] and Mavrikakis et al. [61] have revealed that the pivotal parameter for the reactivity is the relative location of the d-band centre in relation to the Fermi level. An extensive use of the idea of the d-band centre has been accepted as a measure for the characterization of activity of solid metals. Fig. 10 presents the projected density of states onto the d-band of Ag and Pt clusters. The d-band centre of Pt cluster
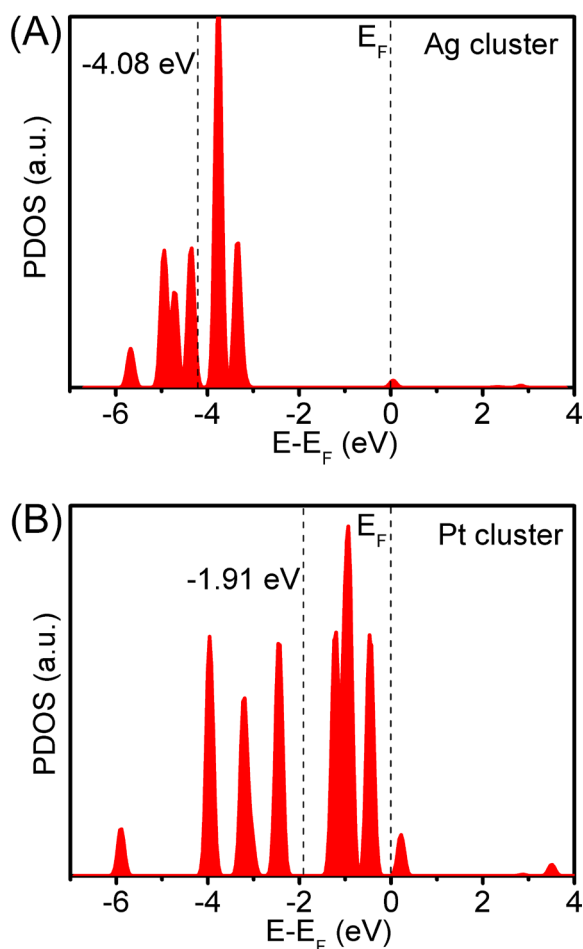
Fig.10. Projected density of state (PDOS) onto d-band of Ag (A) and Pt (B) clusters.

Table 1
Comparison of H_2-generation rate, d-band center and photocurrent for the pure g-C_3N_4, Ag/g-C_3N_4, and Pt/g-C_3N_4 samples

Photocatalyst	H_2-generation rate (µmol g^{-1} h^{-1})	d-band center (Ag, Pt) (eV)	Photocurrent (µA/cm²)
Pure g-C_3N_4	0	~	0.1
Ag/g-C_3N_4	305	−4.08	0.4
Pt/g-C_3N_4	841	−1.91	~0.9
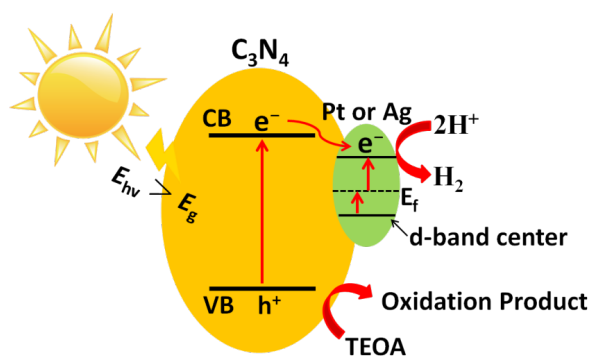
Fig. 11. Schematic diagram on the photocatalytic mechanism for H_2 generation over Pt/g-C_3N_4 or Ag/g-C_3N_4.

(−1.91 eV) is closer to the Fermi level than that of Ag cluster (−4.08 eV), which is consistent with the results obtained by Hammer and Norskov [62], and is recognized that the closer to the Fermi level of the d-band center, the greater the activity, due to making it quite convenient to provide electrons. So, this is one of the main reasons why Pt/g-C_3N_4 possesses a bigger photocurrent and higher photocatalytic activity in water splitting than that of Ag/g-C_3N_4, as shown in Table 1.

3.11. Reaction mechanism

Fig. 11 shows a possible photocatalytic mechanism for Pt/g-C_3N_4 and Ag/g-C_3N_4 in photocatalytic water splitting to H_2 generation. On the irradiation of the Pt/g-C_3N_4 photocatalyst by the simulated sunlight, electrons are excited to g-C_3N_4 CB while holes leave at VB. The CB edge of g-C_3N_4 is higher than the Fermi level of Pt [63], so, the photoexcited electrons on g-C_3N_4 CB are expected to dominate the Schottky barrier, and transferring to the Fermi level of Pt, which results in increasing in the segregation of e$^-$-h$^+$ pairs. The coordination band developed between Pt and g-C_3N_4 is expected to increase the conductivity of g-C_3N_4, also enhancing the electrons transfer from g-C_3N_4 to Pt. It is important that it is the electrons transfer from the g-C_3N_4 to Pt that results in the Pt

Fermi level more negative [64].Therefore, loading of Pt not only speeds up the electron transformation, but also increases the separation efficiency of photogenerated e$^-$-h$^+$ pairs. With regard to the Ag/g-C_3N_4 photocatalyst, the reaction mechanism is quite similar, but the d-band centre of Ag is farther away (more negative) from the Fermi level than that of Pt, the ability of Ag cluster provide electrons to g-C_3N_4 is weaker than that of Pt. So, Pt/g-C_3N_4 shows a higher photocatalytic activity for the water splitting than that of Ag/g-C_3N_4.

4. Conclusion

In this work, Pt or Ag NPs modified g-C_3N_4 nanosheets has been successfully prepared via a simple liquid-phase reduction method. Pt or Ag NPs uniformly adsorbed on the g-C_3N_4 surface, the size of Pt NPs was between 8 and 10 nm and the size of Ag NPs was between 10 and 20 nm. Loading of Ag or Pt can enhance the visible light absorbance of g-C_3N_4, and also improve the photocatalytic efficiency on the water splitting into H_2 generation under simulated sunlight irradiation. Particularly, the loading Pt NPs brings to the higher photocatalytic rate of H_2 generation (841 µmol/g/h for Pt/g-C_3N_4 and 305 µmol/g/h for Ag/g-C_3N_4), while there is almost no H_2 generation for pure g-C_3N_4. Pt as a co-catalyst is better than that of Ag, due to the d-centre of Pt is closer to Fermi level than that of Ag on the g-C_3N_4 surface, which can promote the charge separation and accelerate the electron transformation. This investigation reveals that Pt/g-C_3N_4 constitutes a high active photocatalyst for the water splitting, and developing hydrogen energy.

Notes

The authors declare no competing financial interest.

References

[1] Z. Yan, S. Gong, L. An, L. Yue, Z. Xu, Enhanced catalytic activity of graphene oxide/CeO_2 supported Pt toward HCHO decomposition at room temperature, React. Kinet. Mech. Catal., 124 (2018) 293–304.

[2] Y. Zhao, Y. Wei, X. Wu, H. Zheng, Z. Zhao, J. Liu, J. Li, Graphene-wrapped Pt/TiO_2 photocatalysts with enhanced photogenerated charges separation and reactant adsorption for high selective photoreduction of CO_2 to CH_4, Appl. Catal. B Environ., 226 (2018) 360–372.

[3] Z. Yan, Z. Yang, Z. Xu, L. An, F. Xie, J. Liu, Enhanced room-temperature catalytic decomposition of formaldehyde on magnesium-aluminum hydrotalcite/boehmite supported platinum nanoparticles catalyst, J. Colloid Interface Sci., 524 (2018) 306–312.

[4] K. Qi, Y. Xie, R. Wang, S.-y. Liu, Z. Zhao, Electroless plating Ni-P cocatalyst decorated g-C_3N_4 with enhanced photocatalytic water splitting for H_2 generation, Appl. Surf. Sci., 466 (2019) 847–853.

[5] L. Wang, S. Wang, H. Fu, Y. Wang, K. Yu, Synthesis of Au nanoparticles functionalized 1D α-MoO_3 nanobelts and their gas sensing properties, NANO: Brief Reports Rev., 13 (2018) 1850115.

[6] K. Qi, S.-y. Liu, M. Qiu, Photocatalytic performance of TiO_2 nanocrystals with/without oxygen defects, Chin. J. Catal., 39 (2018) 867–875.

[7] Z. Wei, Y. Zhang, S. Wang, C. Wang, J. Ma, Fe-doped phosphorene for the nitrogen reduction reaction, J. Mater. Chem. A, 6 (2018) 13790–13796

[8] B. Wang, J. Xia, L. Mei, L. Wang, Q. Zhang, Highly efficient and rapid lead(II) scavenging by the natural artemia cyst shell with unique three-dimensional porous structure and strong sorption affinity, ACS Sustain. Chem. Eng., 6 (2017) 1343–1351.

[9] K. Qi, B. Cheng, J. Yu, W. Ho, Review on the improvement of the photocatalytic and antibacterial activities of ZnO, J. Alloys Comp., 727 (2017) 792–820.

[10] K. Qi, S.-y. Liu, Y. Chen, B. Xia, G.-D. Li, A simple post-treatment with urea solution to enhance the photoelectric conversion efficiency for TiO_2 dye-sensitized solar cells, Sol. Energy Mater. Sol. Cells, 183 (2018) 193–199.

[11] J. Zhou, H. Hou, M. Lin, Y. Su, Y. Lu, J. Zhang, G. Qian, Photocatalytic performance of SiO_2-TiO_2 composite via F-assisted restructure of Ti-bearing slag, Desal. Water Treat., 132 (2018) 157–166.

[12] K. Qi, S. Karthikeyan, W. Kim, F.A. Marzouqi, I.S. Al-Khusaibi, Y. Kim, R. Selvaraj, Hydrothermal synthesis of SnS_2 nanocrystals for photocatalytic degradation of 2,4,6-trichlorophenol under white LED light irradiation, Desal. Water Treat., 92 (2017) 108–115.

[13] S. Abuzerr, M. Darwish, A. Mohammadi, S.S. Hossein, A.H. Mahvi, Enhancement of Reactive Red 198 dye photocatalytic degradation using physical mixtures of ZnO-graphene nanocomposite and TiO_2 nanoparticles: an optimized study by response surface methodology, Desal. Water Treat., 135 (2018) 290–301.

[14] M. Ni, M.K.H. Leung, D.Y.C. Leung, K. Sumathy, A review and recent developments in photocatalytic water-splitting using TiO_2 for hydrogen production, Renew. Sustain. Energy Rev., 11 (2007) 401–425.

[15] A. Kudo, Y. Miseki, Heterogeneous photocatalyst materials for water splitting, Chem. Soc. Rev., 38 (2009) 253–278.

[16] A. Fujishima, X. Zhang, D. Tryk, TiO_2 photocatalysis and related surface phenomena, Surf. Sci. Rep., 63 (2008) 515–582.

[17] A.P. Mbouopda, E. Acayanka, S. Nzali, G.Y. Kamgang, E.B. Njoyim Tamungang, S. Laminsi, D. Richard, Comparative study of plasma-synthesized and commercial-P25 TiO_2 for photocatalytic discoloration of Reactive Red 120 dye in aqueous solution, Desal. Water Treat., 136 (2018) 413–421.

[18] B.R. Shah, U.D. Patel, Reductive photocatalytic decolourization of an azo dye Reactive Black 5 using TiO_2: mechanism and role of reductive species, Desal. Water Treat., 130 (2018) 214–225.

[19] T. Ouyang, Y.-Q. Ye, C.-Y. Wu, K. Xiao, Z.-Q. Liu, Heterostructures composed of N-doped carbon nanotubes encapsulating cobalt and β-Mo_2C nanoparticles as bifunctional electrodes for water splitting, Angew. Chem. Int. Ed., 58 (2019) 1–7.

[20] K. Qi, Y. Li, Y. Xie, S.-y. Liu, K. Zheng, Z. Chen, R. Wang, Ag loading enhanced photocatalytic activity of g-C_3N_4 porous nanosheets for decomposition of organic pollutants, Frontiers in Chemistry (2019) DOI:10.3389/fchem.2019.00091.

[21] L. Bo, H. Han, H. Liu, Influence of water quality on photocatalytic degradation of trace carbamazepine in real water bodies, Desal. Water Treat., 124 (2018) 240–247.

[22] W. Zhang, Y. Dong, C. Li, Effects of calcination temperature on photocatalytic degradation of ofloxacin on $Gd_2Ti_2O_7$/HZSM-5, Desal. Water Treat., 126 (2018) 224–230.

[23] M. Khanahmadi, M. Hajaghazadeh, F. Nejatzadeh-Barandozi, F. Gholami-Borujeni, Photocatalytic oxidation process (UV-Fe_2O_3) efficiency for degradation of hydroquinone, Desal. Water Treat., 106 (2018) 305–311.

[24] F. Al Marzouqi, R. Selvaraj, Y. Kim, Thermal oxidation etching process of g-C_3N_4 nanosheets from their bulk materials and its photocatalytic activity under solar light irradiation, Desal. Water Treat., 116 (2018) 267–276.

[25] Q. Xu, B. Zhu, C. Jiang, B. Cheng, J. Yu, Constructing 2D/2D Fe_2O_3/g-C_3N_4 Direct Z-Scheme Photocatalysts with Enhanced H_2 Generation Performance, Solar RRL, 2 (2018) 1800006.

[26] J. Fu, B. Zhu, W. You, M. Jaroniec, J. Yu, A flexible bio-inspired H_2-production photocatalyst, Appl. Catal. B Environ., 220 (2018) 148–160.

[27] M.S. Akple, J. Low, S. Wageh, A.A. Al-Ghamdi, J. Yu, J. Zhang, Enhanced visible light photocatalytic H_2-production of g-C_3N_4/WS_2 composite heterostructures, Appl. Surf. Sci., 358 (2015) 196–203.

[28] K. Qi, B. Cheng, J. Yu, W. Ho, A review on TiO_2-based Z-scheme photocatalysts, Chin. J. Catal., 38 (2017) 1936–1955.

[29] Q. Xiang, J. Yu, M. Jaroniec, Preparation and enhanced visible-light photocatalytic H_2-production activity of graphene/C_3N_4 composites, J. Phys. Chem. C, 115 (2011) 7355–7363.

[30] J. Yu, K. Wang, W. Xiao, B. Cheng, Photocatalytic reduction of CO_2 into hydrocarbon solar fuels over g-C_3N_4–Pt nanocomposite photocatalysts, Phys. Chem. Chem. Phys., 16 (2014) 11492–11501

[31] W.-J. Ong, L.-L. Tan, S.-P. Chai, S.-T. Yong, Heterojunction engineering of graphitic carbon nitride (g-C_3N_4) via Pt loading with improved daylight-induced photocatalytic reduction of carbon dioxide to methane, Dalton Trans., 44 (2015) 1249–1257.

[32] X. Wang, J. Cheng, H. Yu, J. Yu, A facile hydrothermal synthesis of carbon dots modified g-C_3N_4 for enhanced photocatalytic H_2-evolution performance, Dalton Trans., 46 (2017) 6417–6424.

[33] B. Zhu, L. Zhang, B. Cheng, J. Yu, First-principle calculation study of tri-*s*-triazine-based g-C_3N_4: A review, Appl. Catal. B Environ., 224 (2018) 983–999.

[34] J. Fu, Q. Xu, J. Low, C. Jiang, J. Yu, Ultrathin 2D/2D WO_3/g-C_3N_4 step-scheme H_2-production photocatalyst, Appl. Catal. B Environ., 243 (2019) 556–565.

[35] G. Zhang, Z.-A. Lan, X. Wang, Surface engineering of graphitic carbon nitride polymers with cocatalysts for photocatalytic overall water splitting, Chem. Sci., 8 (2017) 5261–5274.

[36] Z. Lu, W. Song, C. Ouyang, H. Wang, D. Zeng, C. Xie, Enhanced visible-light photocatalytic performance of highly-dispersed Pt/g-C$_3$N$_4$ nanocomposites by one-step solvothermal treatment, RSC Adv., 7 (2017) 33552–33557.

[37] F. Fina, H. Menard, J.T.S. Irvine, The effect of Pt NPs crystallinity and distribution on the photocatalytic activity of Pt-g-C$_3$N$_4$, Phys. Chem. Chem. Phys., 17 (2015) 13929–13936.

[38] Y. Fu, T. Huang, L. Zhang, J. Zhu, X. Wang, Ag/g-C$_3$N$_4$ catalyst with superior catalytic performance for the degradation of dyes: a borohydride-generated superoxide radical approach, Nanoscale, 7 (2015) 13723–13733.

[39] M. Ou, S. Wan, Q. Zhong, S. Zhang, Y. Wang, Single Pt atoms deposition on g-C$_3$N$_4$ nanosheets for photocatalytic H$_2$ evolution or NO oxidation under visible light, Int. J. Hydrogen Energy, 42 (2017) 27043–27054.

[40] T. Tong, B. Zhu, C. Jiang, B. Cheng, J. Yu, Mechanistic insight into the enhanced photocatalytic activity of single-atom Pt, Pd or Au-embedded g-C$_3$N$_4$, Appl. Surf. Sci., 433 (2018) 1175–1183.

[41] J. Zhang, M. Grzelczak, Y. Hou, K. Maeda, K. Domen, X. Fu, M. Antonietti, X. Wang, Photocatalytic oxidation of water by polymeric carbon nitride nanohybrids made of sustainable elements, Chem. Sci., 3 (2012) 443–446.

[42] Z. Zhao, Y. Sun, F. Dong, Graphitic carbon nitride based nanocomposites: a review, Nanoscale, 7 (2015) 15–37.

[43] G. Kresse, J. Hafner, Ab initiomolecular-dynamics simulation of the liquid-metal–amorphous-semiconductor transition in germanium, Phys. Rev. B, 49 (1994) 14251–14269.

[44] G. Kresse, J. Furthmiiller, Efficiency of ab-initio total energy calculations for metals and semiconductors using a plane-wave basis set, Comput. Mater. Sci., 6 (1996) 15–50.

[45] J.P. Perdew, J.A. Chevary, S.H. Vosko, K.A. Jackson, M.R. Pederson, D.J. Singh, C. Fiolhais, Atoms, molecules, solids, and surfaces: Applications of the generalized gradient approximation for exchange and correlation, Phys. Rev. B, 46 (1992) 6671–6687.

[46] P.E. Blöchl, Projector augmented-wave method, Phys. Rev. B, 50 (1994) 17953–17979.

[47] G. Kresse, From ultrasoft pseudopotentials to the projector augmented-wave method, Phys. Rev. B, 59 (1999) 1758–1775.

[48] H.J. Monkhorst, J.D. Pack, Special points for Brillouin-zone integrations, Phys. Rev. B, 13 (1976) 5188–5192.

[49] Q. Lin, L. Li, S. Liang, M. Liu, J. Bi, L. Wu, Efficient synthesis of monolayer carbon nitride 2D nanosheet with tunable concentration and enhanced visible-light photocatalytic activities, Appl. Catal. B Environ., 163 (2015) 135–142.

[50] S. Huang, Y. Xu, M. Xie, H. Xu, M. He, J. Xia, L. Huang, H. Li, Synthesis of magnetic CoFe$_2$O$_4$/g-C$_3$N$_4$ composite and its enhancement of photocatalytic ability under visible-light, Colloids Surf. A, 478 (2015) 71–80.

[51] J.-X. Sun, Y.-P. Yuan, L.-G. Qiu, X. Jiang, A.-J. Xie, Y.-H. Shen, J.-F. Zhu, Fabrication of composite photocatalyst g-C$_3$N$_4$–ZnO and enhancement of photocatalytic activity under visible light, Dalton Trans., 41 (2012) 6756–6763.

[52] S. Yang, Y. Gong, J. Zhang, L. Zhan, L. Ma, Z. Fang, R. Vajtai, X. Wang, P.M. Ajayan, Exfoliated graphitic carbon nitride nanosheets as efficient catalysts for hydrogen evolution under visible light, Adv. Mater., 25 (2013) 2452–2456.

[53] T. Chen, W. Quan, L. Yu, Y. Hong, C. Song, M. Fan, L. Xiao, W. Gu, W. Shi, One-step synthesis and visible-light-driven H$_2$ production from water splitting of Ag quantum dots/g-C$_3$N$_4$ photocatalysts, J. Alloys Compd., 686 (2016) 628–634.

[54] E. Liu, L. Kang, F. Wu, T. Sun, X. Hu, Y. Yang, H. Liu, J. Fan, Photocatalytic reduction of CO$_2$ into methanol over Ag/TiO$_2$ nanocomposites enhanced by surface plasmon resonance, Plasmonics, 9 (2013) 61–70.

[55] Y. Hong, Y. Jiang, C. Li, W. Fan, X. Yan, M. Yan, W. Shi, In-situ synthesis of direct solid-state Z-scheme V$_2$O$_5$/g-C$_3$N$_4$ heterojunctions with enhanced visible light efficiency in photocatalytic degradation of pollutants, Appl. Catal. B Environ., 180 (2016) 663–673.

[56] S. Yang, H. Wang, H. Yu, S. Zhang, Y. Fang, S. Zhang, F. Peng, A facile fabrication of hierarchical Ag nanoparticles-decorated N-TiO$_2$ with enhanced photocatalytic hydrogen production under solar light, Int. J. Hydrogen Energy, 41 (2016) 3446–3455.

[57] Y. Yang, Y. Guo, F. Liu, X. Yuan, Y. Guo, S. Zhang, W. Guo, M. Huo, Preparation and enhanced visible-light photocatalytic activity of silver deposited graphitic carbon nitride plasmonic photocatalyst, Appl. Catal. B Environ., 142–143 (2013) 828–837.

[58] Q. Zhai, S. Xie, W. Fan, Q. Zhang, Y. Wang, W. Deng, Y. Wang, Photocatalytic conversion of carbon dioxide with water into methane: platinum and copper(I) oxide Co-catalysts with a core-shell structure, Angew. Chem. Int. Ed., 52 (2013) 5776–5779.

[59] T. Hirakawa, Y. Nosaka, Properties of O$^{2-\bullet}$ and OH$^\bullet$ formed in TiO$_2$ aqueous suspensions by photocatalytic reaction and the influence of H$_2$O$_2$ and some ions, Langmuir, 18 (2002) 3247–3254.

[60] B. Hammer, J.K. Norskov, Electronic factors determining the reactivity of metal surfaces, Surf. Sci., 343 (1995) 211–220.

[61] M. Mavrikakis, B. Hammer, J.K. Nørskov, Effect of strain on the reactivity of metal surfaces, Phys. Rev. Lett., 81 (1998) 2819–2822.

[62] B. Hammer, J.K. Norskov, Theoretical surface science and catalysis—calculations and concepts, Adv. Catal., 45 (2000) 71–129.

[63] H.-S. Wu, L.-D. Sun, H.-P. Zhou, C.-H. Yan, Novel TiO$_2$–Pt@SiO$_2$ nanocomposites with high photocatalytic activity, Nanoscale, 4 (2012) 3242–3247.

[64] G. Liu, K. Du, S. Haussener, K. Wang, Charge transport in two-photon semiconducting structures for solar fuels, Chem. Sus. Chem., 9 (2016) 2878–2904.